Society for Science and Education
United Kingdom

ISSN: 2055 - 1266
Volume 5 No. 1, Feb 2018

Journal of Biomedical Engineering and Medical Imaging

TABLE OF CONTENTS

EDITORIAL ADVISORY BOARD

Prof. Kate N Bishop
The Francis Crick Institute

Prof. Ton Bisseling
Wageningen University

Prof. Anne Blangy
Montpellier University

Prof. Marnie E Blewitt
The Walter and Eliza Hall Institute of Medical Research

Prof. Anna M. Borghi
University of Bologna

Prof. Bettina Böttcher
Bayerische Julius-Maximilians-Universität Würzburg

Prof. Jürgen C Becker
Medical University of Graz

Prof. Laura M Boykin
The University of Western Australia

Prof. Paolo Brambilla
Uinversity of Udine

Prof. Vincenzo Brancaleone
University of Naples Federico II

Prof. Björn Brembs
Universität Regensburg

Prof. Fiona S. Brinkman
Simon Fraser University

Prof. Jon Brock
Macquarie University

Prof. Eoin L. Brodie
Lawrence Berkeley National Laboratory

Prof. Jacqueline Batley
University of Western Australia

Prof. Peter D Baade
Cancer Council Queensland, Australia

DISCLAIMER

All the contributions are published in good faith and intentions to promote and encourage research activities around the globe. The contributions are property of their respective authors/owners and the journal is not responsible for any content that hurts someone's views or feelings etc.

SOCIETY FOR SCIENCE AND EDUCATION UNITED KINGDOM

JBEMi JOURNAL OF BIOMEDICAL ENGINEERING AND MEDICAL IMAGING

ISSN: 2055-1266
VOLUME 5 ISSUE 1

Computed Tomography Image-guided Interaoperative and Stereotactic Calculation Method

Tareq Alhadidi
Medical Equipment Technology Department, College of Applied Medical Sciences, Prince Sattam bin Abdulaziz University, Alkharj, Saudi Arabia
hadidi2@hotmail.com

ABSTRACT

Targeting of deep brain structure pathologies in the operation room and the concept of stereotactic that is applied on the affected zone is described. The achievement of a high accuracy using specialized stereotactic apparatus which controls the surgical tool movement inside the brain is discussed. Calculation of algorithms is necessary for operational planning included. Stereotactic system through combination of hardware-software package which specify the coordinates of surgical zone is designed. Using stereotactic method landmarks during execution of intra-operation by using CT and digital image segmentation are approved and analyzed.

Keywords: Computerized tomography; Physical modeling; Stereotactic method; Stereotactic landmarks; Neurosurgery Simulation.

1 Introduction

Parkinson's disease is a chronic mobility disorder disease. In 1912, the Lirche carried out a kind of cervical rhizotomy in order to treat Parkinsonian tremor. Consequently, several attempts of surgical intervention to control certain types of movement disorders [1-3]. Other specialists also investigated several methods that target the basal ganglia to treat locomotion disorders [4, 5].

The stereotactic surgery was well-established conceptually in advance to the wide utility of several stereotactic frame apparatuses [7,8]. Furthermore, the Russian anatomist Zernov [6] innovated a map of the human intra-cerebral cortex in 1890 interrelated with the main brain functional fields. The basic function of stereotactic apparatus depends on the concept of local effect on a certain intra-cerebral target. This concept can be considered as using specialized stereotactic equipment, intra-scope visualization system, and calculation algorithms can be used for preoperative planning purposes. For getting the perfect performance of stereotactic equipment, first of all we have to perform accurate geometrical parameters calculation "target's coordinates" for the surgical intervention zone.

Before the advent of reconstructive techniques of brain mapping, the initial data for performing stereotactic calculations were components of cerebral ventricles system: this initial data obtained during the carrying out of orthogonal ventriculography in the frontal and sagittal projections [9, 10, and 13]. The geometrical constructions and the calculations include: (1) the calculation of stereotactic

DOI: 10.14738/jbemi.51.4179
Publication Date: 28th February 2018
URL: http://dx.doi.org/10.14738/jbemi. 51.4179

coordinates of intra-cerebral system using brain ventricle landmarks system, (2) modeling of surgical intervention zone by anatomical slices from specialized stereotactic atlases [18], (3) setting of control parameters of the stereotactic apparatus, and (4) calculation of the correction coefficient to reduce the distortion of X-ray images.

Although the universal use of a mentioned technique, this method is somewhat invasive, therefore, from the mid-eighties of the last century, attempts were made to use computerized tomography (CT) and magnetic resonance imaging (MRI) for stereotactic targeting (coordinate determination) [11-17], but the task is complicated by the fact that on the CT-images, it is impossible to conduct differential visualization of sub-cortical structures. The mechanism of scanning and image formation complicates determining standard stereotactic landmarks (and that is necessary for carrying out the calculations). Using of a "new" stereotactic landmarks method which contrastingly visible on topographic slices, often cause accuracy reduction of surgical intervention zone calculation [15].

Therefore, the main issue at the present stage is to solve the problem of adaptation of high informative equipment for intra-cerebral structures mapping, and make the methods of stereotactic calculations based on the brain ventricle landmarks generally accepted.

In this study, there is a description about a universal technique of stereotactic calculations using computed tomography as a tool for intra-operation visualization based on the stereotactic surgical systems applied to 27 patients with ''Parkinson's disease'', the stereotactic surgical system allows for operative maneuvers to be simulated on a simulation software before being implemented on the actual surgical intervention in the operation room. The three-dimensional surgical navigation improves surgical accuracy and can help convert a virtual surgical plan to the operative setting.

2 Experiments and Analysis

CT stereotactic calculations are performed on the basis of neurosurgical department of the Kharkov Regional Hospital while executing surgical intra-operation used a computed tomography CT MAX 3000 General Electric and stereotactic apparatus designed by Edward I. Kandel which allow modeling of polar coordinate system (two angles and one free translational degree for surgical instrument movement). When scanning, the patient lying in supine position, arms resting along the body, the head must secure well in the head holder, support lower legs, and the CT scan protocols is: Sequence Scan mode, Rotation time is 1.0s, Scan time is 1.0s. The stereotactic apparatus fastening is carried out through a fixation of carrying platform inside 25 mm diameter burr hole by using a collar clamp (in our work we did not use massive metal mounting frame).

2.1 The work task

The stereotactic calculation is considered as a high-precision guidance of a surgical instrument to the stereotactic target. For this purpose, the following must be considered:

- Create a virtual model of the human brain for neurosurgical simulation.
- Matching of brain coordinate systems, CT-slice and stereotactic apparatus.
- Determination of reference landmarks on intra-scope images.
- Formation of intra-cerebral stereotactic coordinate system.
- Calculation of the geometric characteristics of the surgical intervention zone.

- ❖ Formation of control parameters for the stereotactic apparatus.

Also while matching the coordinate systems at the initial stage of the procedure; it is necessary to strictly fix the patient's head in the apparatus's scanner gantry by using the following conditions:

i. Stereotactic apparatus platform is mounted perpendicularly to the sagittal or frontal plane of CT-images coordinate system.
ii. Fixation of X-ray contrast marks on the patient's head to ensure of the parallel scanning position of orbit meatal plane.
iii. Determination of craniography obtained by frontal and sagittal projections.

CT-slices under the above scanning conditions are shown in Fig. 1. (Divergence Compensation of X-rays is carried out with software developed by our team). CT-slices on sagittal (Cg) and frontal (F) planes are shown, respectively, in (a) and (b).

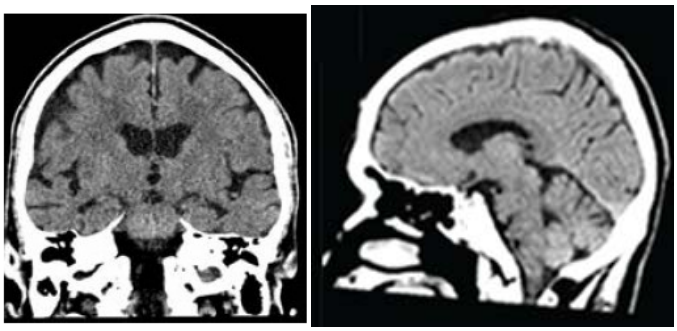

A) B)

Figure 1. CT-slices calculation.

2.1.1 Subsystem visualization and target recognition

Parkinson's disease structure which will be a subject of destruction or simulation (target) is characterized by metastasis state (cervical lymph node). The contrast of this structure is unclear and cannot be visualized from CT-slice using standard method. In this case, using indirect method of visualization for surgical zone (Parkinson's disease), will link the coordinate zone of the target to a reference landmark points inside the center of the brain (the central point between a line that connect anterior-posterior points of the III ventricle). For that we developed an algorithm for finding the central intra-cerebral coordinate system as our reference points which are used for targeting zone by average values. Usually for such landmarks anterior (CA) and posterior (CP) intra-cerebral white adhesions are used (Fig. 3(b)) which are typically defined by III ventricle contours in sagittal and frontal projections.

The basis by scanning is the orbit meatal line (o-m) (skull plane figure 3,a) which passes through the line connects the posterior edge and external auditory meatus parallel to the middle line of (CA-CP) adhesion (by angle of deviation less than 5°). Therefore, from the CT configuration of the III ventricle (V3) (see Fig. 2a), the calculation method for (CA and CP) using axial slice is seen as a sequential scanning of it is region with 1mm step, paralleled to orbit meatal plane. The target (V3) is the length measuring and identification of the slice which contains the second local zone (when identified from top) of the minimum local zone length of (V3) [slide number 3 in Fig. 2 (b)]. In accordance to the scan conditions,

the horizontal CT-slice which contains a specified local minimum length of (V3) will be located in the stereotactic horizontal zero plane.

2.1.2 Determination of (CA and CP) line:

Thus, the task of contrasting landmark determination (CA and CP) will lead us to (V3) length calculation (the distance between anterior and posterior points of V3 contour center) in the studied and selected slice, which contains the second local zone (when identified from the top) of the minimum local zone length of (V3). For stereotactic coordinates CA (FCA, CgCA, GCA) and CP (FCP, CgCP, GCP) we take the coordinates of a central point sequentially to the top and bottom of the current slice contours (V3), taking in account the importance of finding the correct location of (CA and CP). In order of objective evaluation for (V3) length determination we use automatic algorithm for contour recognition based on image processing (segmentation and computer morphometry), for differentiating contours by thresholding image segmentation of target region (Fig. 3(a)) and construction of a binary function characteristic (Fig. 3(b)) by applying differential calculations for V3, and finally we get a colorless zone with clearly contour, and these latter considered as our reference point (Fig. 3(c)).

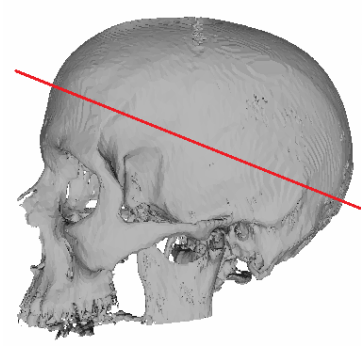

Fig. 2a.

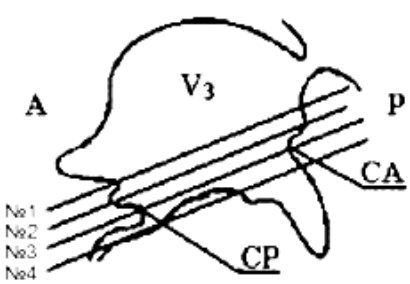

Fig. 2b.

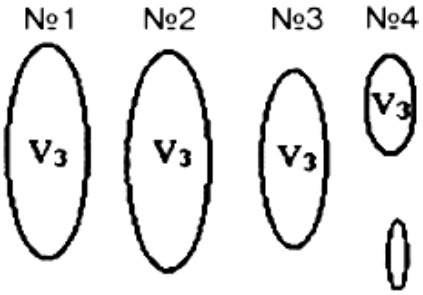

Fig. 2c.

Fig. 2a- Scanning technique used for orbit mental line calculation, 2b- Configuration topological anatomical graph for (V3) finding in sagittal plane, 2c- Horizontal slide parallel to orbit meatal plane.

III ventricle contour determination:

The captured image contains many false contour objects and is extremely difficult for logical interpretation. In this work a combined method is applied to edge the contour: 1) by separating the object from the background, 2) by using of a logical filtration and 2-dimensional differentiation for the resulting 2-D image. Based on the fact that the area of interest (see Fig. 2b) contains one large object (with low contrast) on the color background, the segmentation is carried out by the method of threshold binarization . The histogram of such image (see Fig. 2c) has clearly pronounced bimodal character and has interactively threshold (can be execution manually) is not difficult. The Automation of such histogram analysis in order to select the two largest maxima peaks is not a trivial task and was carried out using the following algorithm:

1. smoothing the Linearity of the histogram for the purpose of blocking minor vibrations by using the following formula:

$$\overline{S_i} = \frac{1}{K+1} \sum_{j=-K}^{K} S_{i+j}, 1+K \le i \le 255-K, \quad (1)$$

Where S_i - histogram values at i^{th} contrast level, $\overline{S}_i$ - averaged values, K - number of previous and subsequent points near the point with an index i. The smoothing effectiveness when studying the contrast data distributions was implemented at the values of K ≥ 7.

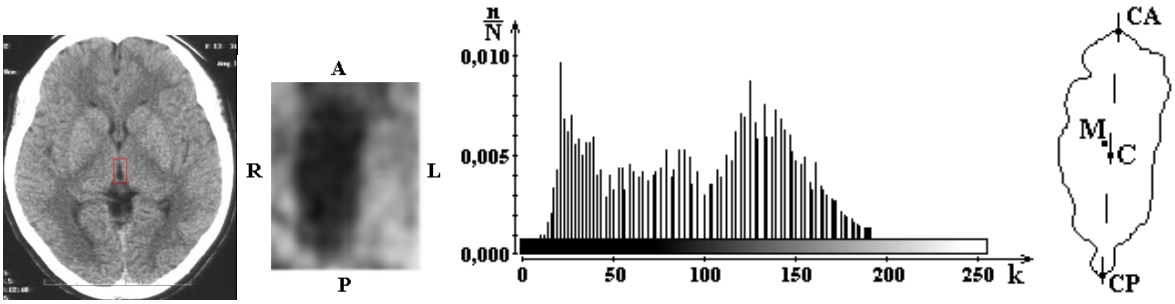

Fig.3a. Fig. 3b. Fig. 3c. Fig. 3d.

Figure. 3 figure shows an automatic algorithm for (V3) finding and contour recognition.

(a) Axial tomographic slice at zero stereotactic horizontal plane,

(b) Target zone;

(c) Histogram of the processed area;

(d) Resulting contour image of (V3).

2. Finding local maxima in the smoothed histogram according to the following condition:

$$\max_{i\in[0;255]} \left\{ \begin{array}{l} \overline{s}_0 \ge \overline{s}_{i+1}; \\ \vec{s}_{i-1} \le \overline{s}_i \ge \overline{s}_{i+1}, \quad 1 \le i \le 254; \\ \overline{s}_{255} \ge \overline{s}_{i-1}. \end{array} \right\} \quad (2)$$

By introducing additional conditions to the algorithm we can find a maximums flat peak on the smoothed histogram.

The threshold is selected as the mean value between the two maxima (the standard one and the maximum local, it is not located near the standard maximum). The false objects are eliminated with the help of a logical filter, taking into account the connectivity and regions size.

The resulting 2-D image that contains the object and the background was obtained using 2-dimensional differentiation operators based on the tabulating the calculation of the gradient G, specified by contrast function f(x,y) :

$$\| G \| = | f(x+1, y) - f(x, y) | + | f(x, y+1) - f(x, y) | \quad (3)$$

(CA-CP) centering:

After that, constructing the straight line connecting the two spikes CA-CP, and finding the coordinates center of (V3) mass M(x_M , y_M) is done. This coordinates are determined by the formula:

$$x_M = \frac{\sum_{i=1}^{N_o} x_i}{N_o}, \quad y_M = \frac{\sum_{i=1}^{N_o} y_i}{N_o} \tag{4}$$

Where N_o - the number of points belongs to the object (V3).

The center of intra-cerebral stereotactic coordinate system is point C (Fc, Cgc, Gc), located in the mid-line connecting the adhesion line (CA-CP), which are calculate according to the formulas:

$$F_c = \frac{F_{CA} + F_{CP}}{2}; Cg_c = \frac{Cg_{CA} + Cg_{CP}}{2}; G_c = \frac{G_{CA} + G_{CP}}{2} \tag{5}$$

Zero frontal stereotactic planes pass through the central point which perpendicular to the line (CA-CP); zero sagittal stereotactic plane passes through a line (CA-CP), perpendicular to the frontal and horizontal planes. Central point of stereotactic coordinates of surgical intervention zone is M (F, Cg, G) which is determined according to point (C) which is determined according to anatomical slices data from the brain atlases. CT-slices in zero horizontal plane (Fig. 4a) calculated by frontal (F) and sagittal (Cg) stereotactic coordinates, and the horizontal coordinate (G) is determined by a general slice in sagittal projection (Fig. 4b). The visualization of a sagittal plane (Cg) displaced from point (M) is carried out by a general slice scan on the frontal projection (Fig. 4c). Next, the affine transformation of an intra-cerebral coordinate is performed, target points in CT-images system is carried out by using a parallel displacement and rotation of coordinate axes. The parameters (1F, 1Cg, 1G) determine the distance from point (M) to the reference bone landmarks (at the external bone walls, the contours which are visualized in most clearly) which facilitates linking of coordinates.

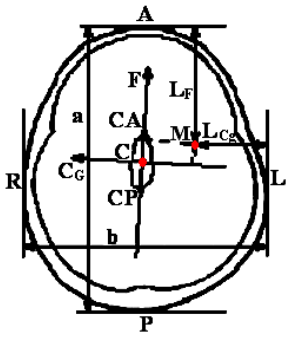

Fig. 4a.

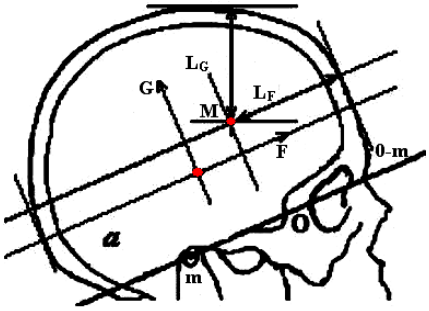

Fig. 4b.

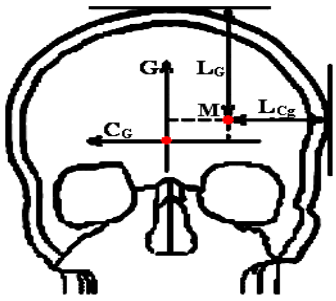

Fig. 4c.

Fig. 4a- Schematic diagram of CT-slice on zero level stereotactic horizontal planes.
Fig. 4b- Schematic diagram of general image in stereotactic sagittal plane.
Fig. 4c- Schematic diagram of general image in stereotactic frontal plane.

The calculation of surgical instrument orientation based on Kandel stereotactic apparatus. The coordinates of surgical intervention zone is verified by functional control equipment.

2.1.3 Stereotactic to target movement

Since the orbitomeatal line parallel to the line (CA–CP) the deviation angle is not more than (5˚) [11], horizontal CT-slice which contains the minimum length of local zone (V3) is located in a zero horizontal stereotactic plane (Figure 5c). Zero frontal stereotactic planes passes through the center point perpendicular to a line (CA-CP). Zero sagittal stereotactic planes passes through the line (CA-CP) perpendicular to the frontal and horizontal planes. Stereotactic coordinates for a central point of surgical zone M (F′, Cg′, G′) are determined according to point (C), according to anatomical data-slices from brain atlases, and the most perfect of them is the atlas [18]. The determination of individual variability of brain structures can be done by volumetric coefficients. The final stage of surgical intervention zone visualization is the reconstruction of intra-cerebral coordinate zone for target-point into a tomography image coordinates, and that can be achieved by transferring and rotating coordinate's axes, considering the opposite direction of the sagittal axis (see Fig. 5).

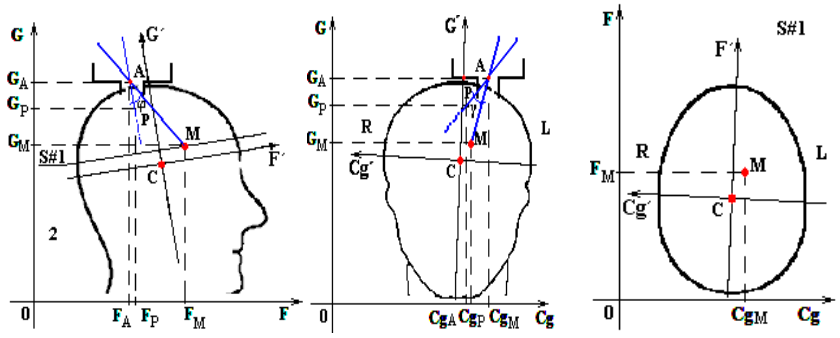

Fig. 5a. Fig. 5b. Fig. 5c.

Figure. 5, Surgical-zone visualization (intra-cerebral coordinates zone), and the position of target's point determination.

The calculation of orientation parameters for a surgical instrument movement inside the brain is carried out by a pre-movement with a value of (rP ≈ 15÷20 mm) toward the target , and this allows visualization of a CT-plane of the surgical instrument projection in sagittal and frontal planes. Taking into account the known coordinates of the rotation center of the stereotactic apparatus A (FA, CgA,GA) for the target zone M (FM, CgM, GM) and the current position of the distal tip of surgical instrument P (FP, CgP,GP) and the rotation angles (ϕ) and (γ) in the sagittal plane (Fig. 5a) and the frontal plane (Fig. 5b), as well as the surgical instrument movement toward the depth (rM) relative to the point (A), we can use the following formulas:

$$tg\varphi = \left|\frac{k_2 - k_1}{1 + k_1 k_2}\right|, \quad tg\gamma = \left|\frac{k_4 - k_3}{1 + k_4 k_4}\right| \tag{6}$$

$$r_M = \sqrt{(F_A - F_M)^2 + (Cg_A - Cg_M)^2 + (G_A - G_M)^2} \tag{7}$$

Where:

к1, к2, к3, к4 – the angular coefficients of straight lines connecting between the current position of surgical instrument distal tip and target in relation to the rotation center of the stereotactic apparatus:

$$k_1 = \frac{G_A - G_M}{Cg_A - Cg_M}, \qquad k_2 = \frac{G_A - G_P}{Cg_A - Cg_P} \tag{8}$$

$$k_3 = \frac{G_A - G_M}{F_A - F_M}, \qquad k_4 = \frac{G_A - G_P}{F_A - F_P} \tag{9}$$

Thus the additional depth movement of the surgical instrument (rX) taking into account the preliminary depth inside the brain, is:

$$r_X = r_M - r_P. \tag{10}$$

3 Results and discussion

The ability of calculation of additional depth movement for the surgical instrument has extreme importance especially when dealing with a multiple surgical guidance. Thus to apply the method, a software was designed to allow visualization of surgical-intervention zone and for formation of the control parameters of stereotactic apparatus in a surgical instruments guidance.

While using the surgical planning method which applied on 27 patients, the total error of a surgical instrument targeting was less than 3 mm (in average 2.6 mm) compared with others systems. Stereotactic calculations were performed using a developed, calculating graphical software that allows visualization of zone of surgical intervention and forming the control parameters of stereotactic apparatus for guiding the surgical instruments. An intra-operation by using CT-stereotactic calculations applying stimulating electrode into the sub-thalamic zone located 2 mm laterally, and 10 mm posterior and 3 mm ventral from center (F = -1.2, Cg = 10.91, G = -6.23) sub-thalamic nucleus: CT-slice at stereotactic zero-plane is shown on (Fig. 6a):

1 – The calculation of coordinates at central surgical zone,

2 – Shot-screen for cannula movement in CT-slice forward surgical intervention zone (Fig. 6b),

3 – Distal point of cannula at the active part.

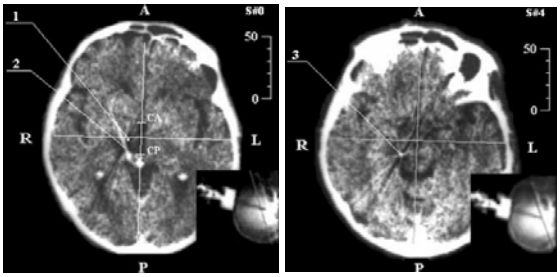

Fig. 6a. Fig. 6b.

Figure. 6- Demonstration of neurosurgery CT-stereotactic calculation, while targeting the med-nucleus with colorless ball: a). stereotactic CT-slice at zero-plane level, b). CT- stereotactic calculation at the level of surgical zone: 1. The calculation of central point stereotactic-target zone, 2. Artifact of cannula movement, 3. Distal point of the cannula moving part.

4 Conclusions

The aim of this work is to develop a virtual model of the human brain that could be used in a neurosurgical simulation for preoperative planning purposes. In order to obtain a realistic and useful simulation we focused our study on the physical modeling of the brain targeting (med-nucleus colorless body) and on the maneuvers of the surgical instruments. The study included the following:

1. The study methodology provides high accuracy to identify orbit meatal plane for the skull which is necessary for reference stereotactic landmark determination.
2. The visualization of (V3) contours which is necessary to localize the center of intra-cerebral stereotactic coordinate system.
3. Using the proposed method, it clinically increased the accuracy of stereotactic operations in parkinsonian disease by (30%).
4. Furthermore, increasing the accuracy of stereotactic-guidance in functional surgery is associated with increasing of the accuracy of ability of the reconstruction techniques of CT-image for obtaining 3D-image and the development of algorithms machine of intro-scope data analysis for full-automatic recognition of the intra-cerebral landmarks taking into account their variation. Also the surgical operations planning system must be improved to allow performing virtual volumetric simulation of the main stages of surgical intervention.

REFERENCES

[1] Carroll, William M.. International Neurology. John Wiley & Sons. p. 188. ISBN 9781118777367. Archived from the original on 8 September 2017.

[2] Fingar KR, Stocks C, Weiss AJ, Steiner CA (December 2014). Most Frequent Operating Room Procedures Performed in U.S. Hospitals, 2003–2012"

[3] Sveinbjornsdottir, S . The clinical symptoms of Parkinson's disease. Journal of Neurochemistry. 139:p 318–324. https://www.ncbi.nlm.nih.gov/pubmed/27401947

[4] Fitzgerald, M; Bellgrove M; Gill, M. Handbook of Attention Deficit Hyperactivity Disorder. John Wiley & Sons. p. 270.

[5] Santosh, Paramala J; Henry, Amy; Varley, Christopher K (24 January 2008). "ADHD and hyperkinetic disorder". In Peter Tyrer; Kenneth R. Silk. Cambridge Textbook of Effective Treatments in Psychiatry. Cambridge University Press. p. 782. ISBN 978-1-139-46757-5.

[6] Zernov D. L'encephalometre. Rev Gen Clin Ther 1890; 19:302.

[7] Carlson, Neil R."Physiology of Behavior".Pearson Education, Inc., 2013. p.134..

[8] Paddick, I. A simple dose gradient measurement tool to complement the conformity index. Journal of Neurosurgery. P 105: 194–201. PMID 18503356. https://www.ncbi.nlm.nih.gov/pubmed/18503356

[9] De Salles, A. Radiosurgery from the brain to the spine: 20 years' experience. Acta Neurochirurgica Supplements. 101: p 163–168. https://www.ncbi.nlm.nih.gov/pubmed/18642653

[10] Kavanagh, B. D.. Extracranial radiosurgery (stereotactic body radiation therapy) for oligometastases. Seminars in radiation oncology. 200616 (2): p 77–84. https://www.ncbi.nlm.nih.gov/pubmed/16564443

[11] Verellen, D. Innovations in image-guided radiotherapy". Nature Reviews. Cancer. 7 (12):p 949–960.

[12] Shershever A. et al. Calculation of target destruction using MRI, during stereotactic-endoscopic microsurgical techniques. Journal of neurosurgery issues. Institute of Neurosurgery named after academician N.N.Burdenko — 2001. — №3. — p:24–25.

[13] Grunert P., Darabi K., Espinosa J., Filippi R, Computer-aided navigation in neurosurgery, Neurosurgery. Rev. — 2003. — V.26, N2. — P.73–99. https://www.ncbi.nlm.nih.gov/pubmed/12962294

[14] Han J.K., Hwang P.H., Smith T.L. Contemporary use of image-guided systems, Curr. Opin. Otolaryngol. Head Neck Surg, 2003. — V.11, N1. — P.33–36. https://www.ncbi.nlm.nih.gov/pubmed/14515099

[15] Iacopino D.G, Conti A, Angileri F.F, Tomasello F, Different methods for anatomical targeting, Journal of Neurosurgery Science. 2003..47, P.18–25. https://www.ncbi.nlm.nih.gov/pubmed/12900728

[16] Athos, J. and Storm, DR. High Precision Stereotaxic Surgery in Mice. Current Protocols in Neuroscience. 2001. A.4A.1–A.4A.9. https://www.ncbi.nlm.nih.gov/pubmed/18428449

[17] Nakao N., Nakai K., Itakura T. Updating of Neuro-navigation based on images intra-operatively acquired with a mobile computerized tomographic scanner. Technical note, Minim. Invas. Neurosurg. 2003 V.46, N2 P.117–120.

SOCIETY FOR SCIENCE AND EDUCATION UNITED KINGDOM

JBEMi JOURNAL OF BIOMEDICAL ENGINEERING AND MEDICAL IMAGING

ISSN: 2055-1266
VOLUME 5 ISSUE 1

Mobile Three Gas Extractor Using Pressure Swing Adsorption Method

Pascalin Tiam Kapen [1, 2], Tendong Tadadjeu Neville [1], Dongmeza Koudjou Jauspin [1]
[1]Université des Montagnes, ISST, Bangangté-Cameroon
[2]University of Dschang, IUT-FV, LISIE/L2MSP, Bandjoun-Cameroon
fpascalin20022003@gmail.com; tadadjeuneville@yahoo.fr; dkjauspin@gmail.com

ABSTRACT

This paper deals with a simple approach of producing three gases that are oxygen, nitrogen and pressurized air by using a mobile three gas extractor. Indeed, the proposed medical device integrates the following modules driven by an Arduino Mega 2560 board: Module of filtration and production of air made of filters, compressor and a cooling coil; module of oxygen and nitrogen production based on pressure swing adsorption (PSA) method and using the zeolite molecular sieves that restrain nitrogen and produce oxygen. The device is equipped of pressure sensors to control the output pressure of the gases. This implemented equipment has been tested and we obtained promising results. Indeed, a percentage of oxygen of 82 % has been reached. We have produced pressurized air with a pressure of 2.5 bars.

Key words: Mobile Tree Gas Extractor; Oxygen; Nitrogen; Pressurized Air; Pressure Swing Adsorption (PSA).

1 Introduction

The supply of oxygen, nitrogen and pressurized air is a major problem in hospitals in developing countries [1, 2]. The usefulness of these gases is no longer to demonstrate. Indeed, oxygen is used for patients suffering from hypoxia; nitrogen is used for the conservation of physiological fluids like blood and many devices work with pressurized air. It is therefore interesting to start thinking about a simple equipment capable of producing such gases. It is in this vein, that we propose a simple mobile three gas extractor using pressure swing adsorption method.

2 Material and methods

2.1 Material

The electronic components used in our work are made of:

- Two filters, for the elimination of air particles having a diameter more than 2.5 micro-meters or less than 2.5 micro-meters ;
- A compressor used for bringing up the pressure of air at 3 bars;

DOI: 10.14738/jbemi.51.4238
Publication Date: 3rd March 2018
URL: http://dx.doi.org/10.14738/jbemi. 51.4238

- A cooling coil used for cooling the pressurized air;
- Two molecular sieves used to trap nitrogen and produce oxygen;
- A PT100 temperature sensor, used for measuring the temperature of oxygen;
- Three HK 3023 pressure sensors, for measuring the pressure of various gases;
- A pressure regulator, used in regulating the pressure of the compressed air, that is 3 bars, to the atmospheric pressure that is 1.01325 bar;
- An oxygen sensor, used in measuring the concentration of oxygen;
- A flow meter, used in regulating the flow of oxygen;
- A humidifier, used in humidifying oxygen given to the patient;
- An ATMEGA 2560 microcontroller card for commanding the entire system;
- Valves, used for commanding air, nitrogen and oxygen circulation.

The operating diagram of our equipment is shown in figure 1:

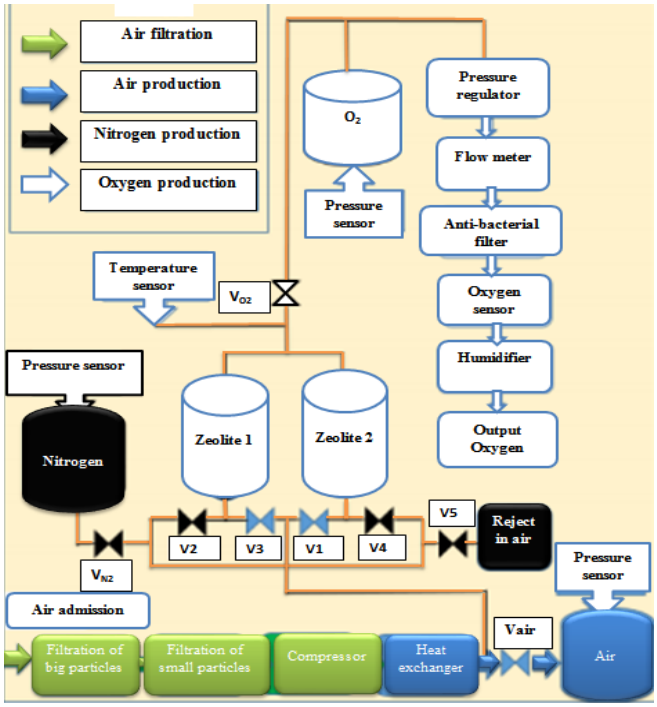

Figure 1 : Operating diagram

Where

V_{N2}, V_2 and V_4 are the electrical valves admitting the flow of Nitrogen;

V_{O2}, V_3 and V_1 are the electrical valves admitting the flow of Oxygen;

V_{air} is the electrical valve admitting the flow of pressurized air.

The Arduino Mega 2560 board driving the different modules is presented in figure 2.

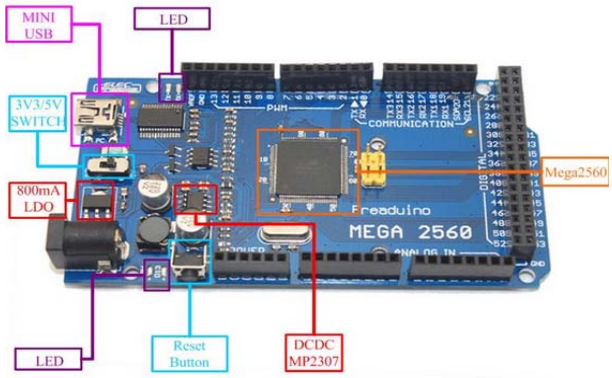

Figure 2 : Arduino Mega 2560 board

The electronic card incorporating the Arduino Mega 2560 board and developed in this work can be visualized in figure 3.

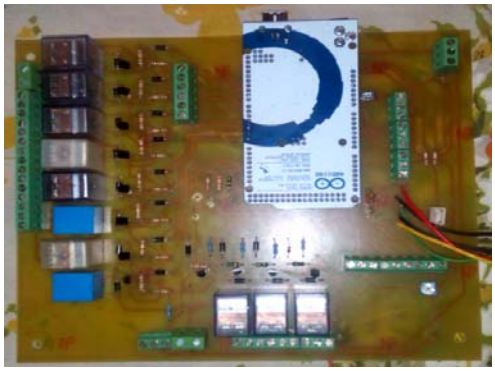

Figure 3: Electronic card commanding all the modules

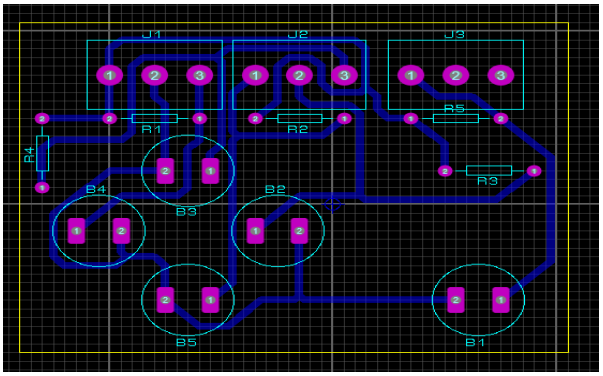

Figure 4: ARES circuit of the electronic card commanding all the modules

2.2 Methods

2.2.1 Module of filtration and production of pressurized air

The filtration of air is provided by two filters, one for restraining particles of more than 2.5 micro-meters of diameter and the other one used for restraining particles of less than 2.5 micro-meters of diameter. A compressor is used for elevating the pressure of air till 3 bars. Then a cooling coil is used for cooling the air till the atmospheric temperature. We use a pressure sensor to control the pressure of air.

2.2.2 Module of production of oxygen

In order to produce oxygen, the pressure swing adsorption (PSA) method has been implemented. Indeed, the approach consists of the production of oxygen passes through the usage of two zeolite molecular sieves. These sieves are used to restrain nitrogen molecules and produce oxygen. A PT100 temperature sensor has been used to measure the temperature of oxygen produced, in order to secure the patient. In addition, a pressure regulator has been used for regulating the pressure of air from the value of 3 bars to the value of 1.1325 bar. An oxygen sensor has been incorporated for to measure of

oxygen concentration. A flow meter is used for regulating the flow of oxygen and a humidifier for humidifying the gas administrated to the patient.

2.2.3 Module of production of nitrogen

By injecting the oxygen at the outlet of zeolite molecular sieves, nitrogen restrained by the zeolite is liberated and can be stored in a tank.

2.2.4 Module of display on an LCD screen 20*4

We used an LCD screen 20*4. The information displayed is:

- Oxygen temperature;
- Oxygen pressure;
- Pressurized air pressure.

3 Results and discussion

Our equipment was tested and we obtained promising results.

3.1 Module of filtration and production of pressurized air

We made a test by using a HK 3023 pressure sensor in order to control the pressure of the pressurized air at the outlet of our circuit. The result is shown is figure 5.

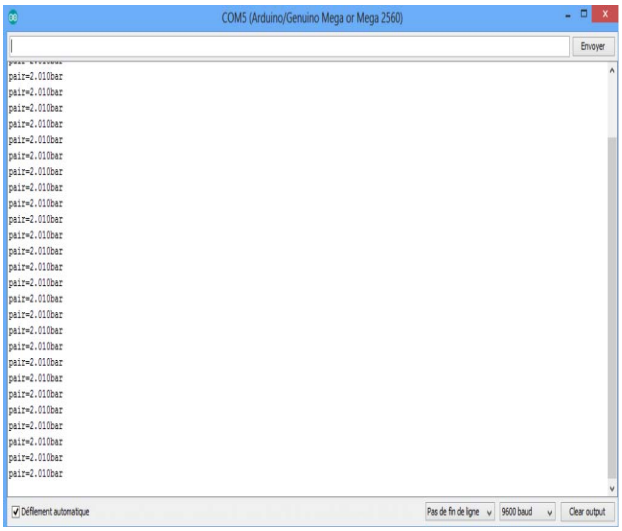

Figure 5: Screenshot showing the pressurized air pressure evolution from the serial monitor of the Arduino Mega 2560 board

3.2 Module of production of oxygen

The oxygen temperature and pressure are visualized from a serial monitor of the Arduino Mega 2560 board by using a PT100 temperature sensor and a HK 3023 pressure sensor. The results are presented in figures 6 and 7.

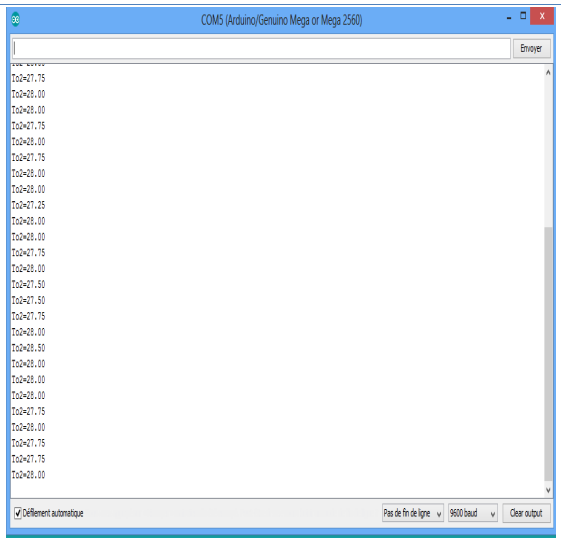

Figure 6: Screenshot showing the oxygen temperature evolution from the serial monitor of the Arduino Mega 2560 board

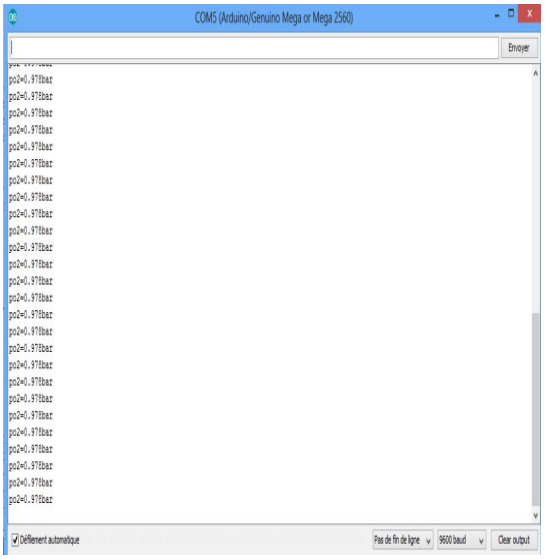

Figure 7: Screenshot showing the oxygen pressure evolution from the serial monitor of the Arduino Mega 2560 board

Figure 8: Test of oxygen concentration

An oxygen concentration (between 82 % and 95 %) obtained with the equipment is shown on the LCD screen in figure 8.

The final equipment developed in this work is presented in figure 9.

Figure 9: Different views of the final equipment

4 Conclusion

In this paper, a mobile three gas extractor using pressure swing adsorption method has been developed. Indeed, the equipment developed consisted of a module of filtration and production of air made of filters, compressor and a cooling coil; a module of oxygen and nitrogen production based on pressure swing adsorption (PSA) method and using the zeolite molecular sieves that restrain nitrogen and produce oxygen. It can be concluded that the implemented medical device produced a good percentage of oxygen between 82 % and 95 %. In addition, a pressure of 2.5 bars has been reached for the pressurized air. It would be useful to improve the equipment by adding a hybrid enery supplier in case of electrical power failure. It would be also important to reinforce a security system. All this constitutes the ways of investigation of future works.

REFERENCES

[1] Mullie, A. (2010). Les gaz à usage médical, des produits thérapeutiques pas comme les autres: aspects spécifiques de l'application de la législation pharmaceutique, de son enregistrement à sa distribution (Doctoral dissertation).

[2] Organisation mondiale de la Santé (2016). Spécifications techniques pour les concentrateurs d'oxygène.

SOCIETY FOR SCIENCE AND EDUCATION UNITED KINGDOM

JBEMi JOURNAL OF BIOMEDICAL ENGINEERING AND MEDICAL IMAGING

ISSN: 2055-1266
VOLUME 5 ISSUE 1

Strain Elastography & Tissue Characterization as a Tool to Differentiate Tumor from Healthy Tissue

Mahdi Al-Qahtani, Omar Altuwaijri and Ravish Javed
Biomedical Technology Department, College of Applied Medical Sciences, King Saud University, Riyadh, KSA
amahdi@ksu.edu.sa; oaltwijri@ksu.edu.sa; ravish.javed@yahoo.com

ABSTRACT

The purpose of this study was to compare diagnostic values of normal and effected tissues with two techniques using strain elastography and tissues characterization. This study was carried out on a breast phantom containing all human body parameters. Analysis was performed using a lone phantom to correlate a relation between the values of Strain Elastography (SE) and first order texture parameters results. For SE SonixTouch Q+ (Ultrasonix Medical Corporation, 130-4311 Viking Way, Richmond, Canada) device using a linear-array ultrasound probe at a frequency of 10MHz with a gain of 40%. Elastography breast phantom was purchased from CAE healthcare USA, 3600 Edgelake Drive Sarasota FL, USA. For tissue characterization a Region of Interest (ROI) that encompasses both (normal and stiffer) areas were selected. MAZDA software was used to carry out the image analysis (mean and variance) of the tumour and healthy tissue, ROI of 1600 pixels at both regions was selected. An affirmative and resilient outcome was observed between the numerals of normal and tumor tissues, both for SE and first order texture parameters values. After our study we suggest that SE and tissue characterisation via first order texture parameter is a reliable technique to highlight normal and tumor tissue (with respect to same reference, for SE technique only). SE and first order texture parameters (mean and variance) paved way in highlighting the breast tumors fully. It is suggested that SE being more reliable approach in determining the stiffness for breast lesion, as it produces the results with real time imaging. However texture parameter gives an objective assessment of the image with a discriminating feature of the tissue.

Keywords: Elastography, Texture analysis, Breast, Tumor.

1 Introduction

Cancer in breast is one of the most common cause of death among women worldwide [1]. Breast tumor frequency has increased rapidly in recent years, it is the most common pathological formation towards breast cancer [2]. During reproductive years, its incidence increases in particular and after 50 years of age with a slower rate (average age of menopause) [3]. Occurrence rates of breast cancer are high in women across developed countries in contrast to less developed countries, but frequency of incidence rates are also increasing in less developed countries [3]. About 2.7% of women in Europe and North

DOI: 10.14738/jbemi.51.4246
Publication Date: 12th March 2018
URL: http://dx.doi.org/10.14738/jbemi. 51.4246

America suffers from breast cancer by age of 55, whereas 5.0% by age of 65 and around 7.7% by age of 75 [4].

Variation in pliability of tissues is ascribed to pathological condition [5]. Tissue elasticity changes due to numerous circumstances, among cancerous tissues appear as hard lumps due to density increased, whereas other tissues disorders encompasses deposition due to fat or collagen. In conventional ultrasound examination cysts containing fluid may not be visible. A diminished superficial lesion or pathological abnormality departs undetected via traditional ultrasound in several cases [6]. Conventional ultrasound is based on qualitative technique [7], though to differentiate healthy tissues from the diseased there was a need to establish a quantitative approach. The ultrasound elastography was introduced to overcome this issue.

Elastography is a non-invasive medical imaging technique. It analyses stiffness of effected tissue region when compared to other normal tissue as per the image, based on this comparisons it detects tumours. Numerous imaging mode of ultrasound is been used for the most common type of elastography to equate the shape of the tissue under examination before and after it is compressed slightly. As cancerous tissue tends to be stiffer than normal tissue. Image obtained by elastogram shows different shades of light and dark, with different degree of stiffness. Several tumours are detected with elastogram, including breast tumor better than traditional ultrasonic images. Elastography use a small uniform compression on the tissue that provides insight of the elastic properties of the tissue [8].

Two basic types of elastography are currently performed; strain elastography (SE) and shear wave elastography (SWE) [9]. SE is observed by applying strain manually by the user and establishing the relative strain in a tissue with comparisons to its surrounding tissue [10, 11]. Whereas, SWE simply uses a combination of shear waves, it measure the absolute value of the tissue and delivers tissue elasticity based on force values detected by the machine [12, 13].

Recent studies have demonstrated SE techniques individually for various tissues. However, till date their results are not studied and supported via texture parameters in particular. Here we report the evaluation of breast tumor with healthy tissue in a phantom using SE and institute a link by analyzing the image via first order texture parameter.

2 Material and Methods

2.1 Study design

This study was conducted in the Biomedical Technology Department in accordance with guidelines followed by ethical review board of King Saud University. A breast phantom was utilized for the study containing all human body parameters. Analysis was performed using a lone phantom to correlate a relation between the values of SE and first order texture parameters results.

2.2 Ultrasound examination

B-Mode ultrasound on breast phantom was performed with using SonixTouch Q+ (Ultrasonix Medical Corporation, 130-4311 Viking Way, Richmond, Canada) device using a linear-array ultrasound probe at a frequency of 10MHz with a gain of 40%. Elastography breast phantom was purchased from CAE healthcare USA, 3600 Edgelake Drive Sarasota FL, USA. The breast phantom ultrasound examination was

performed via previously described guidelines as per The World Federation for Ultrasound in Medicine and Biology (WFUMB) [14].

2.3 Elastographic strain ratio

Elastography mode was selected to measure strain ratio on two different regions on the phantom, tumour and adjacent normal tissue with a common normal tissue (tissue A) as a reference within the phantom was castoff to measure strain ratios. Primarily strain ratio for tumour was calculated by taking a region on interest (ROI) positioned in the tumour with tissue A. Furthermore for calculating the second strain ratio another ROI normal tissue (adjacent to tumour) was also examined with same tissue A.

2.4 Image acquisition

A set of one best image within the range of strain sensor from a cine loop of 99 images were picked. In each image 5 random areas were selected for strain ratios, initially for tumour then adjacent healthy tissue with respect to a common tissue A as shown in figure 1. To increase reliability elastographic strain ratios were repeated in 5 successive sessions, with atleast a 2-hours interval.

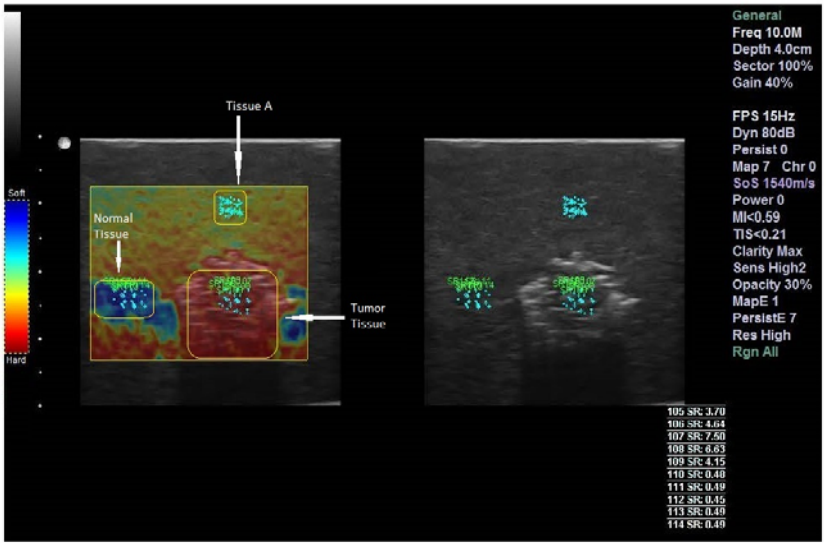

Figure 1 Elastographic and B-Mode image of breast phantom with Normal, Tumor and Tissue A (as reference).

2.5 First order texture parameters

To correlate the tumour and healthy tissue on the breast phantom an ROI that encompasses both the areas were selected. MAZDA version 4.5 software (Institute of Electronics, Technical University of Lodz, Poland) was used to perform the texture feature extraction, it permits calculation of the texture features suggested in the available literature. To carry out the image analysis of the tumor and healthy tissue, ROI of 1600 pixels at both regions was selected. All 5 images at both (normal and stiffer) sections were analysed for mean and variance with same ROI. The intensity of the signal of each ROI was normalized using the limitation of dynamics to $\mu \pm 3\sigma$ (μ, gray-level mean; and σ, gray-level standard deviation).

2.6 Statistical analysis

The data obtained from texture parameter were analysed with SPSS version 2 software (IBM Corporation, Armonk, NK). One way ANOVA was utilized to ascertain the significant difference between the values. Statistical significance was set at P equal 0.05.

3 Results

An affirmative and resilient outcome was observed between the numerals of normal and tumor tissues, both for SE and first order texture parameters values.

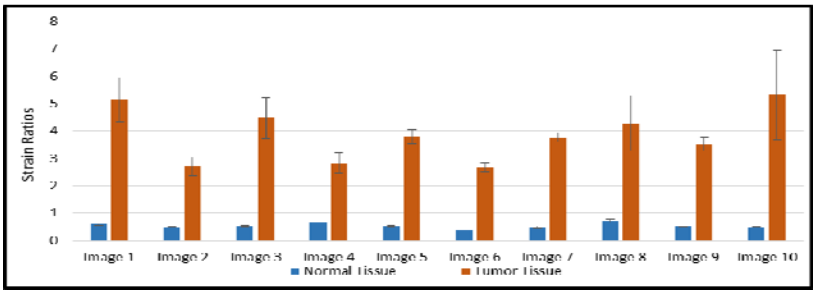

Figure 2 Strain ratios of individual images of normal tissue with respect to tumor.

Figure 2 represents strain ratios of each image using ultrasound elastography technique with persistent trend of superior stiffness in the tumor region in contrast to normal tissue. Image 10 showing the highest strain ratios, whereas Image 2 & 6 showing the lowest value of stiffness in tumor.

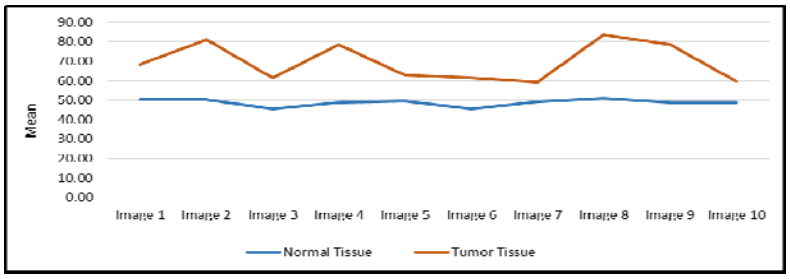

Figure 3 Mean values of each image with normal and tumor tissues.

Figure 3 depicts the mean values of each image for both the tissues (normal and tumor) via using first order texture parameters. The mean value from texture parameter illustrates irregularity in value of hardness of tumour tissue when compared to normal tissue.

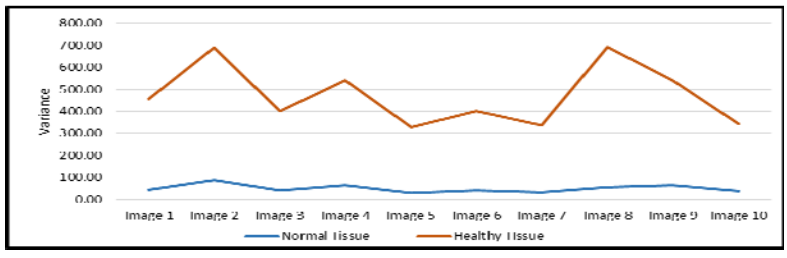

Figure 4 Variance values of individual image with normal and tumor tissues.

Figure 4 displays the values of variance for each image encompassing normal and tumor tissues through first order texture parameters. A significant difference and indiscretion in values of tumour tissues was perceived when associated with normal tissue.

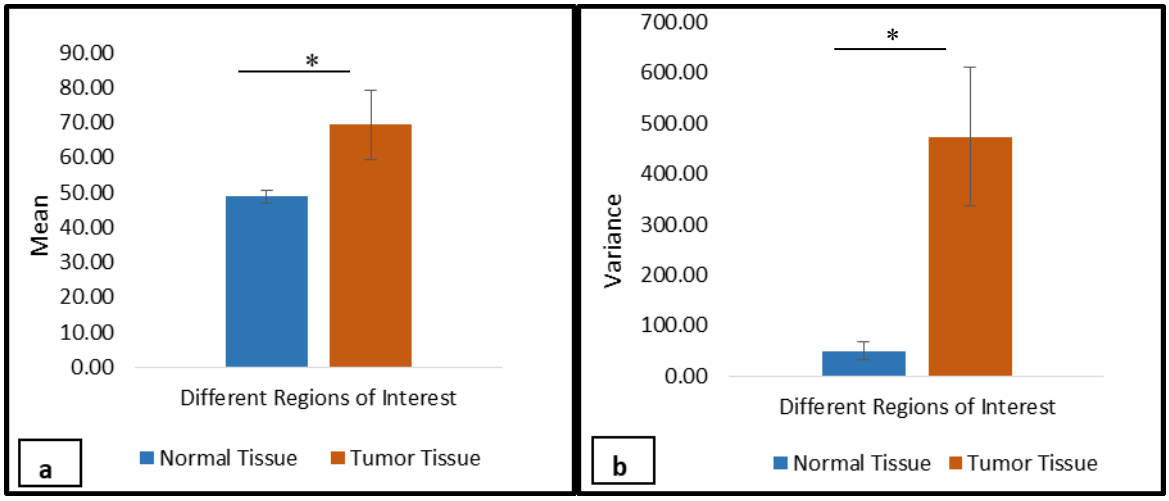

Figure 5 (a) Cumulative mean values of normal and tumor tissues. (b) Cumulative variance values of normal and tumor tissues. ** Showing significant difference between values of tissues.*

Figure 5 a & b illustrates the cumulative mean and variance values of all the images consisting normal and tumor tissues, respectively. As seen evidently both the figure show a higher value of mean and variance for tumor tissue when compared to normal tissue.

4 Discussion

Lesion in breast lump is a common disorder paving way for tumors. Often these tumor can get malignant and if not separated from breast and can transform to cancer in breast [15]. Imaging is evident for evaluation purposes when there are obstinate or perplexing symptoms [16-18]. SE and magnetic resonance imaging are the most extensively used techniques for identifying the pathological status of the tumor. SE is a practical and non-invasive method. Furthermore, with the introduction of high frequency transducers has ensued in better visual appearance of the superficial organs and especially soft tissues [19]. The results of SE are the imaging methodology with higher reliability and accuracy. To determine deviation in hyperechoic areas for swelling, tears, lesions and calcifications in tissues with the help of SE using high-frequency transducers is quite successful. Though, conventional ultrasound imaging is yet to advance the desired accuracy rates as SE in displaying out the abnormalities. SE exhibits a comparative value of strain in contrast to the surrounding area [20]. This approach is achieved in real-time with either manually or automatically compressing the desired tissue [21, 22]. Sensation practice is widely used since decades to perceive stiffness change in a tissue. SE also work on the origin of sensation [9]. For calculating the stiffness through SE two ROI's are selected to display the value. Notable studies are already been performed on breast, liver, thyroid and other tissues [23-27]. SE is user dependent and occasionally variations in result are also common [28].

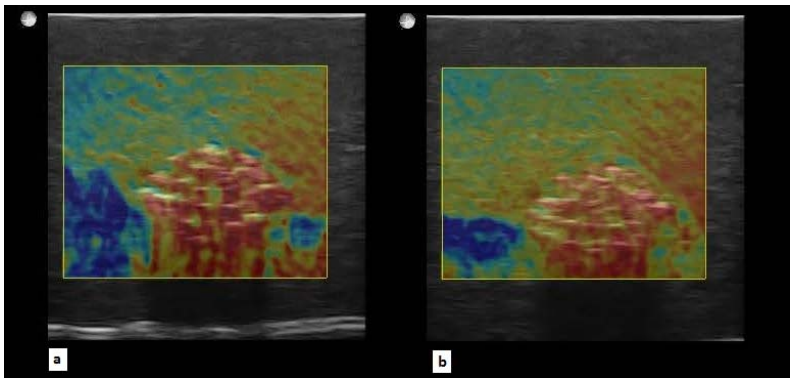

Figure 6 a & b Two different elastographic image of same phantom with clear visual difference.

As we can see in figure 6 a & b shows two different elastographic images of the same breast phantom. As perceived from the images in figure 6 a & b there is a slight variation in values of strain ratios as well as different visual pattern of normal and tumor tissues. Despite the difference in values both the figures are clearly showing tumor as red in colour with higher stiffness while soft tissue can be seen with blue colour with lesser stiffness.

Texture parameters studies have been conducted on various instances for numerous body parts images. However texture parameter studies on breast phantom consolidating SE was falling short. Here we determine first order texture parameters by analysing the values of mean and variance show remarkable difference among normal and tumor tissue, also assisting the values of strain ratios for both the tissues (normal and tumor). A higher significant difference value of variance was detected for normal and tumor tissue, whereas a low significant difference value of mean was observed.

After our study we suggest that SE and tissue characterization via first order texture parameter is a reliable technique to highlight normal and tumor tissue (with respect to same reference, for SE technique).

5 Conclusion

SE and first order texture parameters (mean and variance) paved way in highlighting the breast tumors fully. It is suggested that SE being more reliable approach in determining the stiffness for breast lesion, as it produces the results with real time imaging. However texture parameter gives an objective assessment of the image with a discriminating feature of the tissue.

Current study was exercised on a breast phantom containing all human body parameters. It is recommended that future studies must be conducted on females suffering from tumor in breast with respect to surrounding normal tissue, to measure the strain ratio for stiffness with suitable external reference with values of mean and variances for first order texture parameter.

ACKNOWLEDGEMENT

The authors would like to extend their appreciation to the College of Applied Medical Sciences Research Center and the Deanship of Scientific Research at King Saud University for funding this research.

REFERENCES

[1] Murray, C.J. and A.D. Lopez, *Mortality by cause for eight regions of the world: Global Burden of Disease Study.* The lancet, 1997. 349(9061): p. 1269-1276.

[2] Carter, C.L., C. Allen, and D.E. Henson, *Relation of tumor size, lymph node status, and survival in 24,740 breast cancer cases.* Cancer, 1989. 63(1): p. 181-187.

[3] Key, T.J., P.K. Verkasalo, and E. Banks, *Epidemiology of breast cancer.* The lancet oncology, 2001. 2(3): p. 133-140.

[4] Cancer, C.G.o.H.F.i.B., *Breast cancer and hormone replacement therapy: collaborative reanalysis of data from 51 epidemiological studies of 52 705 women with breast cancer and 108 411 women without breast cancer.* The Lancet, 1997. 350(9084): p. 1047-1059.

[5] Krouskop, T.A., et al., *Elastic moduli of breast and prostate tissues under compression.* Ultrasonic imaging, 1998. 20(4): p. 260-274.

[6] Ophir, J., et al., *Elastography: a quantitative method for imaging the elasticity of biological tissues.* Ultrasonic imaging, 1991. 13(2): p. 111-134.

[7] Manning, F.A., C.M. Hill, and L.D. Platt, *Qualitative amniotic fluid volume determination by ultrasound: antepartum detection of intrauterine growth retardation.* American journal of obstetrics and gynecology, 1981. 139(3): p. 254-258.

[8] Ophir, J., et al., *Elastography: ultrasonic estimation and imaging of the elastic properties of tissues.* Proceedings of the Institution of Mechanical Engineers, Part H: Journal of Engineering in Medicine, 1999. 213(3): p. 203-233.

[9] Bamber, J., et al., *EFSUMB guidelines and recommendations on the clinical use of ultrasound elastography. Part 1: Basic principles and technology.* Ultraschall in der Medizin-European Journal of Ultrasound, 2013. 34(02): p. 169-184.

[10] Vural, M., et al., *The evaluation of the retrobulbar orbital fat tissue and optic nerve with strain ratio elastography.* Medical ultrasonography, 2015. 17(1): p. 45.

[11] Park, H., et al., *Strain elastography features of epidermoid tumours in superficial soft tissue: differences from other benign soft-tissue tumours and malignant tumours.* The British journal of radiology, 2015. 88(1050): p. 20140797.

[12] Cortes, D.H., et al., *Continuous shear wave elastography: a new method to measure viscoelastic properties of tendons in vivo.* Ultrasound in Medicine and Biology, 2015. 41(6): p. 1518-1529.

[13] Athanasiou, A., et al., *Feasibility of imaging and treatment monitoring of breast lesions with three-dimensional shear wave elastography.* Ultraschall in der Medizin-European Journal of Ultrasound, 2017. 38(01): p. 51-59.

[14] Barr, R.G., et al., *WFUMB guidelines and recommendations for clinical use of ultrasound elastography: Part 2: breast.* Ultrasound in Medicine and Biology, 2015. 41(5): p. 1148-1160.

[15] Rickert, R.R., L. Kalisher, and R.V. Hutter, *Indurative mastopathy: a benign sclerosing lesion of breast with elastosis which may simulate carcinoma.* Cancer, 1981. 47(3): p. 561-571.

[16] Gordon, P.B. and S.L. Goldenberg, *Malignant breast masses detected only by ultrasound. A retrospective review.* Cancer, 1995. 76(4): p. 626-630.

[17] Hayes, R., M. Michell, and H. Nunnerley, *Acute inflammation of the breast—the role of breast ultrasound in diagnosis and management.* Clinical Radiology, 1991. 44(4): p. 253-256.

[18] Houssami, N., et al., *Sydney Breast Imaging Accuracy Study: comparative sensitivity and specificity of mammography and sonography in young women with symptoms.* American Journal of Roentgenology, 2003. 180(4): p. 935-940.

[19] Rizzatto, G., et al., *High-resolution sonography of breast carcinoma.* European journal of radiology, 1997. 24(1): p. 11-19.

[20] Al-Qahtani, M., *Shear-Wave and Strain Elastography: A Comparative Review on Principles, Basic Techniques and Applications.* Current Medical Imaging Reviews, 2016. 12(4): p. 269-278.

[21] Cho, N., et al., *Sonoelastographic strain index for differentiation of benign and malignant nonpalpable breast masses.* Journal of Ultrasound in Medicine, 2010. 29(1): p. 1-7.

[22] Hiltawsky, K.M., et al., *Freehand ultrasound elastography of breast lesions: clinical results.* Ultrasound in Medicine and Biology, 2001. 27(11): p. 1461-1469.

[23] Al-Qahtani, M., et al., *A Comparative Study of Shear-Wave Elastography and Strain Elastography on a Breast Phantom for Diagnosis of Tumor and Cyst.* Journal of Biomedical Engineering and Medical Imaging, 2015. 2(3): p. 24.

[24] Monpeyssen, H., et al., *Elastography of the thyroid.* Diagnostic and interventional imaging, 2013. 94(5): p. 535-544.

[25] Rykhtik, P., et al., *Experience of Using Elastography in the Diagnosis of Liver Fibrosis in the Practice of Hepatology Center.* Radiology, 2015. 1: p. 49.

[26] Nicolas, E., S. Callé, and J.-P. Remenieras, *Generating shear waves in the human brain for ultrasound elastography: a new approach.* Physics Procedia, 2015. 70: p. 1255-1259.

[27] Uramoto, H., et al., *Intraoperative ultrasound elastography has little diagnostic benefit for deeper tumours of the lung.* European Journal of Cardio-Thoracic Surgery, 2015. 49(5): p. 1538-1539.

[28] Fleury, E.d.F.C., et al., *New elastographic classification of breast lesions during and after compression.* Diagnostic and Interventional Radiology, 2009. 15(2): p. 96.

